High Field-Emission Stability of Offset-Thin-Film Transistor-Controlled Al-Doped Zinc Oxide Nanowires

2011 Jpn. J. Appl. Phys. 50 04DN07

(http://iopscience.iop.org/1347-4065/50/4S/04DN07)

Japanese Journal of Applied Physics **50** (2011) 04DN07 **REGULAR PAPER**
DOI: 10.1143/JJAP.50.04DN07

High Field-Emission Stability of Offset-Thin-Film Transistor-Controlled Al-Doped Zinc Oxide Nanowires

Po-Yu Yang*, Jyh-Liang Wang[1], Wei-Chih Tsai[2], Shui-Jinn Wang[3], Jia-Chuan Lin[4], I-Che Lee, Chia-Tsung Chang, and Huang-Chung Cheng

Department of Electronics Engineering and Institute of Electronics, National Chiao Tung University, Hsinchu 30010, Taiwan
[1]*Department of Electronics Engineering, Ming Chi University of Technology, Taipei 24301, Taiwan*
[2]*Department of Electronic Engineering, National Formosa University, Yunlin 63201, Taiwan*
[3]*Institute of Microelectronics, Department of Electrical Engineering, National Cheng Kung University, Tainan 70101, Taiwan*
[4]*Department of Electronics Engineering, St. John's University, Taipei 25135, Taiwan*

Received September 15, 2010; accepted November 24, 2010; published online April 20, 2011

Aluminum-doped zinc oxide (AZO) nanowire (NW) arrays incorporating an offset thin-film transistor (offset-TFT) have been proposed to achieve high field-emission (FE) stability. The AZO NW field emission arrays (FEAs) were hydrothermally grown at a low temperature of 85 °C. The uncontrolled AZO NW FEAs demonstrated superior FE characteristics (i.e., turn-on field of ~2.17 V/μm and threshold field of ~3.43 V/μm) compared with those of the conventional CNT FEAs grown at a temperature below 600 °C. However, uncontrolled AZO NW FEAs show a larger current fluctuation of 15.6%. Therefore, the offset-TFTs were used to control the AZO NW FEAs. Consequently, the fluctuation of AZO NW FEAs could be significantly reduced to less than 2%. This novel field emission device exhibits good emission stability, low-voltage controllability, low-temperature processing, and structural simplicity, making it promising for applications in flat panel displays.

1. Introduction

Field emission display (FED) has emerged as a leading contender in display technologies, because it combines the analogous features of cathode ray tubes (CRTs) and flat panels. The field emitters provide cold electrons to bombard phosphors in an anode plate to generate high luminance. In the last decade, various one-dimensional (1D) nanomaterials with high aspect ratios have been intensively investigated for field emitter arrays (FEAs).[1–4] Among these candidates, carbon nanotubes (CNTs) have attracted considerable attention as a field emission source owing to their small tip radii of curvature, high electrical conductivity, good chemical inertness, and high mechanical strength.[5–8] However, Fowler–Nordheim (FN) field emission (FE) is very sensitive to the work function of the emitter surface and the nanometer structure of the emitter, giving rise to the problems of instability and nonuniformity in anode currents.[9] A long-channel thin-film transistor (LC-TFT, i.e., a TFT with a channel width of 100 μm and channel length of 250 μm) has been used to reduce the current fluctuation and driving voltage of CNT FEAs.[10] Despite this, the LC-TFT occupied a large substrate area and showed drawbacks with respect to fine pixels. Furthermore, the reported CNT FEAs fabricated by microwave plasma-enhanced chemical vapor deposition (MPCVD) with high power (~1500 W) and high substrate temperature (~800 °C) inside a vacuum facility showed seriously degraded field-effect mobility and on/off current ratio of LC-TFT owing to plasma damage and high-temperature processing. The required high temperature and vacuum facility of CNT growth introduce difficulties with respect to the fabrication of large-area FEDs by the direct deposition of CNTs.[11] Hence, the architecture of a high-voltage TFT with integrated Al-doped ZnO (AZO) nanostructure FEAs is suggested to solve these issues of LC-TFT-controlled CNT FEAs. A high-voltage TFT can be realized by an excimer laser crystallization (ELC) technique with an offset design of the undoped region in the drain side, and excellent transistor performance (i.e., high field-effect mobility and on/off current ratio) can be achieved with low-temperature processing and a high-breakdown voltage between the drain and the gate/source can be ensured.[12–14] Recently, AZO nanostructures revealed their potential on the FEAs because of the high conductance and good crystal quality,[15] and they can be expected to have lower turn-on fields and higher anode currents. Moreover, AZO nanostructures can be prepared by hydrothermal methods, which are suitable for FEA fabrication because of the low reaction temperature, low cost, catalyst-free growth, uniform production, large area, and compatibility with plastic electronics.[16] In this study, a complete low-temperature fabrication of offset-TFT-controlled AZO nanostructure arrays is proposed to obtain highly stable FEAs. The accompanying field emission characteristics and current stability of FEAs is systematically addressed.

2. Experimental Procedure

Figure 1 shows the fabrication procedures for offset-TFT-controlled AZO nanostructure FEAs. An amorphous silicon (α-Si) film 100 nm thick was deposited on the oxidized wafer by low-pressure chemical vapor deposition (LPCVD) using a pure SiH_4 gas at 550 °C [Fig. 1(a)]. After standard RCA cleaning, the α-Si thin films were irradiated by a KrF ($\lambda = 248$ nm) ELC system (Lambda Physik LPX 210i). During the laser process, the samples were placed on a substrate in a vacuum chamber with 10^{-3} Torr while the substrate was maintained at room temperature [Fig. 1(b)]. Each irradiated pulse of 30 ns duration delivered a maximum energy density of 400 mJ/cm^2 over an area of 1.8×25 mm^2. The laser beam was homogenized into a semi-gaussian shape along the short axis and a flat-top shape along the long axis. The number of laser shots was 100 with an equivalent overlap of 99%. After laser irradiation, the polycrystalline silicon (poly-Si) film was patterned to form the active region [Fig. 1(c)]. Next, a 300-nm-thick tetraethylorthosilicate silicon dioxide (TEOS–SiO_2) layer and a 200-nm-thick poly-Si layer were deposited using plasma-enhanced chemical vapor deposition (PECVD) at 350 °C and LPCVD at

*E-mail address: youngboy.ee96g@g2.nctu.edu.tw

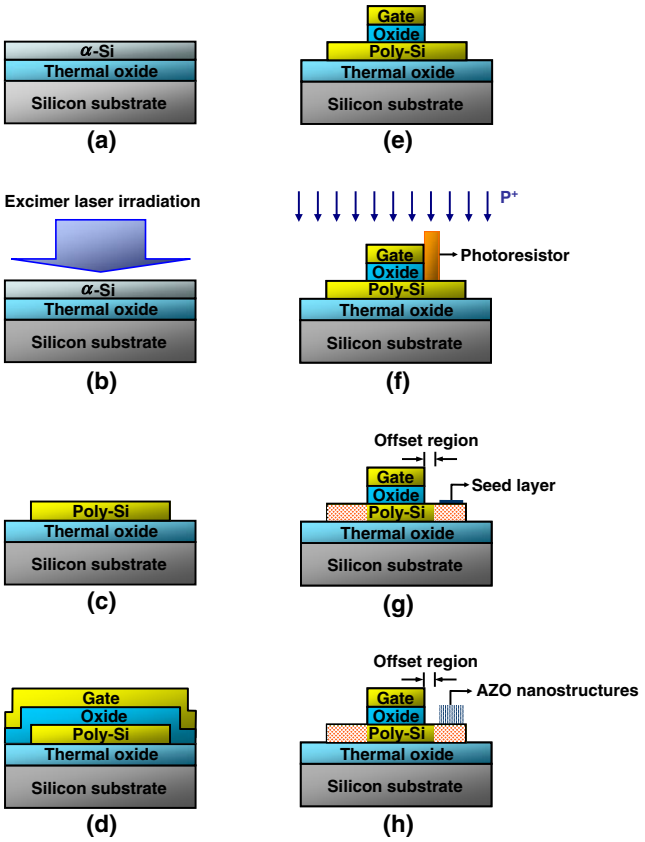

Fig. 1. (Color online) Fabrication procedures for offset-TFT-controlled AZO nanostructure FEAs.

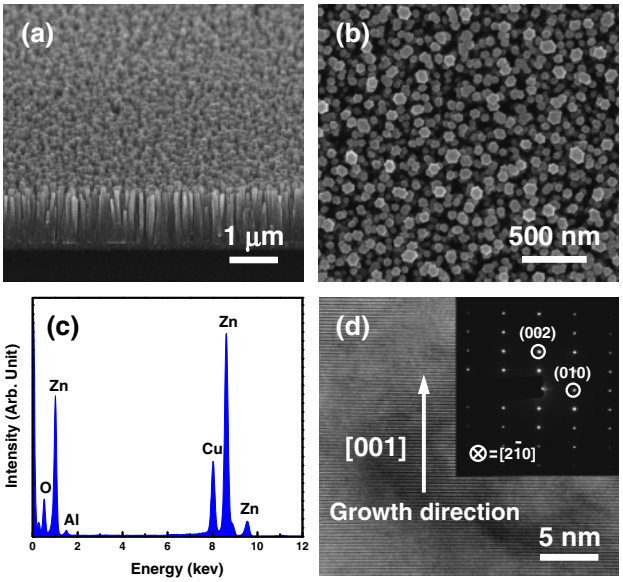

Fig. 2. (Color online) (a) FE-SEM images (45° tilt view) and (b) top view of AZO NW arrays synthesized on the drain region of the offset-TFT. (c) EDS spectrum of the AZO NWs. (d) High-resolution TEM image of AZO NW. The inset is the corresponding diffraction pattern.

550 °C, respectively [Fig. 1(d)]. The poly-Si and oxide layers were then etched to form the gate electrode [Fig. 1(e)]. Afterwards, the offset region was defined with protection using a photoresist. Different offset-region lengths were established. After ion implantation of phosphorus with a concentration of $5 \times 10^{15}\,\mathrm{cm}^{-2}$, a self-aligned source and drain were formed for the offset-TFT [Fig. 1(f)]. To activate the dopant, the sample was annealed at 600 °C for 24 h in N_2 ambient. A sputtered AZO seed layer 200 nm thick with a $1 \times 1\,\mathrm{mm}^2$ square pattern was formed at the drain of the offset-TFT by the lift-off technique [Fig. 1(g)]. Subsequently, AZO NW FEAs were grown selectively on the AZO seed layer by a hydrothermal method at 85 °C for 60 min [Fig. 1(h)]. The precursor solution was prepared by mixing 25 mM zinc nitrate hexahydrate [$Zn(NO_3)_2 \cdot 6H_2O$] and 25 mM hexamethylenetetramine (HMTA) in 300 ml deionized water at room temperature. The 0.77 mM aluminum nitrate nonahydrate [$Al(NO_3)_3 \cdot 9H_2O$] was added as the dopant source into the precursor solution. The samples were thoroughly rinsed with deionized water to eliminate residual salts and dried in air at room temperature.

The morphology of the AZO nanostructures was observed by field-emission scanning electron microscopy (FE-SEM; Hitachi S-4700I). The crystallinity and chemical composition of the samples were investigated by high-resolution transmission electron microscopy (HRTEM; JEOL JEM-3000F) integrated with energy-dispersive X-ray spectroscopy (EDS). The HRTEM samples were prepared by scraping the nanostructures off the substrates, dispersing them in ethanol, and then drop casting them onto holey carbon-coated copper grids. The field emission characteristics of AZO nanostructure FEAs with or without offset-TFT control were analyzed using Kiethley237 high-voltage units through an IEEE 488 interface controlled by a personal computer in a vacuum chamber under 1.0×10^{-7} Torr at room temperature.

3. Results and Discussion

Figure 2(a) presents the FE-SEM images (45° tilt view) of the AZO nanostructure FEAs synthesized on an AZO seed layer. The morphology of AZO nanostructures reveals the shape of nanowires (NWs), which were well ordered and vertically aligned on the AZO seed layer/poly-Si substrate. The AZO NWs are uniformly distributed over the entire area of the AZO seed layer. The top-view FE-SEM image of the AZO NWs is shown in Fig. 2(b). It indicates that the aligned AZO NWs have an average diameter of ∼100 nm and a controllable length of ∼1 μm. The outlines of the NWs can be seen as well-defined hexagons, which may be attributed to the wurtzite structure of ZnO single crystals. In addition, Fig. 2(c) shown the EDS spectrum of NWs validated to the elemental signals of Zn, O, and Al, which are consistent with the elements added in the hydrothermal precursor solution. The TEM analysis was conducted to confirm the crystallinity and orientation of AZO NWs. The HRTEM image in Fig. 2(d) clearly shows a well-resolved lattice image and suggests that the AZO NW is a single-crystalline wurtzite structure with an elongated *c*-axis. The NW growth direction was determined from both the HRTEM image and the selective-area electron diffraction (SAED) pattern. The growth direction was recognized as that along [001], the fastest growth direction of ZnO crystals.

Figure 3(a) shows the transfer characteristics when the offset lengths of TFTs were changed. The leakage current (defined at a gate voltage of −10 V) decreases by approximately five orders of magnitude as the offset length

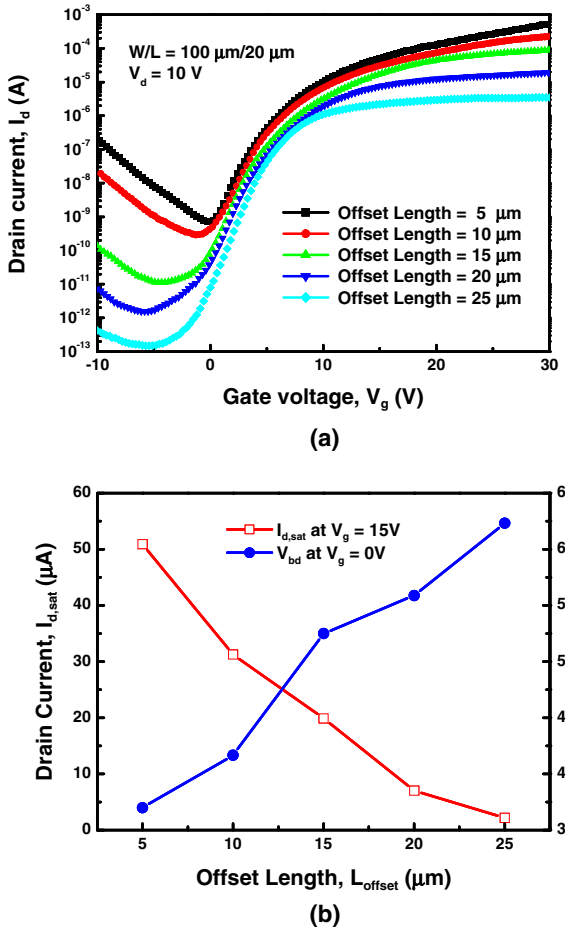

Fig. 3. (Color online) (a) Transfer characteristics of the offset-TFTs with various offset lengths. (b) Breakdown voltages and saturated drain currents for different offset lengths of offset-TFTs.

is increased from 5 to 25 μm. This phenomenon can be connected to the decrease in the electric field in the offset-gate channel region that suppresses the field-enhanced emission from the coulombic traps in Si grain boundaries, resulting in a decrease in the leakage currents between the source and drain as the offset length is increased.[14] Figure 3(b) shows the saturated drain currents ($I_{d,sat}$) and breakdown voltages (V_{bd}) for different offset lengths of offset-TFTs. The $I_{d,sat}$ was determined at a gate voltage (V_g) of 15 V. As can be seen, a higher $I_{d,sat}$ is indicated for a shorter offset length of offset-TFT. In contrast, the breakdown voltage increases with offset length. The breakdown voltage is measured between the source and drain when $V_g = 0$ V. This breakdown phenomenon can be associated with an increasing electric field at the offset channel region while the offset length is decreased. To obtain a reasonable breakdown voltage and a moderate $I_{d,sat}$, the offset-TFT with an offset length of 15 μm was chosen as a control device for the AZO NW FEAs.

Figure 4 illustrates the transfer characteristics of offset-TFTs before and after the hydrothermal AZO NW growth. The electrical properties of the offset-TFTs before and after AZO NW growth are almost the same, revealing field effect mobilities of 48.34 and 48.36 $cm^2/(V \cdot s)$, on/off current ratios of 8.29×10^6 and 8.31×10^6, threshold voltages of 7.37 and 7.33 V, and subthreshold swings of 1.36 and

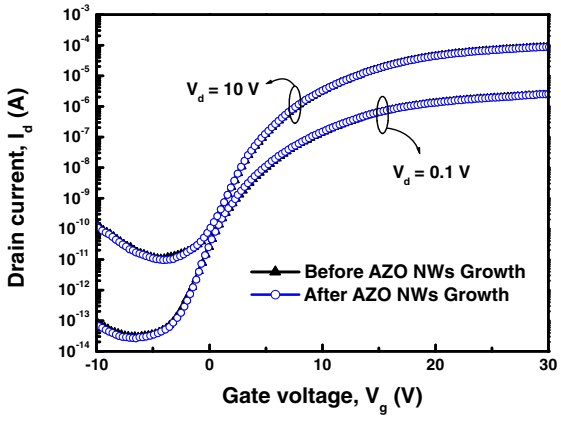

Fig. 4. (Color online) Transfer characteristics of offset-TFTs with offset lengths of 15 μm before and after the growth of AZO NWs.

1.33 V/dec, respectively. In contrast, the reported LC-TFTs suffered serious degradation of field-effect mobility and on/off current ratio owing to plasma damage and high-temperature (i.e., ~800 °C) processing during CNT fabrication.[10] Hence, the process of hydrothermal AZO NW growth at a low temperature (i.e., 85 °C) without plasma damage can be beneficial for the stability of offset-TFTs.

A schematic diagram of the experimental measurement setup is shown in Fig. 5(a). A glass plate coated with indium–tin-oxide (ITO) and phosphor was used as an anode and positioned 100 μm above the sample surface. The field emission properties of the offset-TFT-controlled AZO NW FEAs were characterized in a high-vacuum environment with a base pressure of 1.0×10^{-7} Torr. Figure 5(b) shows field emission characteristics for AZO NW FEAs with and without offset-TFT control. Anode currents (I_a) were measured as a function of anode voltages (V_a) at various gate voltages of offset-TFTs. The turn-on electric field (defined as the field at a current density of 1 $\mu A/cm^2$) and threshold field (estimated as the field at a current density of 1 mA/cm^2) for the uncontrolled AZO NW FEAs are ~2.17 and ~3.43 V/μm, respectively. Normally, the anode current of uncontrolled AZO NW FEAs increased markedly with anode voltage. Compared to the low-temperature CNTs (i.e., grown at 250 to 550 °C),[17–21] the AZO NW FEAs hydrothermally grown at 85 °C in this study demonstrate superior field emission characteristics (i.e., turn-on field of ~2.17 V/μm and threshold field of ~3.43 V/μm) than those (i.e., turn-on field of 2.4 to 3.85 V/μm and threshold field of 4.3 to 6 V/μm) of the reported CNT FEAs, which supports that AZO NW FEAs are good candidates for low-temperature-fabricated FEDs. On the other hand, anode currents were controlled by the offset-TFTs and showed saturated behavior at high anode voltages. Saturated anode currents of 82.4, 197.5, and 397.5 μA were obtained for offset-TFT gate voltages of 15, 20, and 25 V, respectively. This suggests that the anode current can be modulated by the TFT gate voltage. In addition, the turn-on fields of the offset-TFT-controlled AZO NW FEAs were raised to 2.4 V/μm because of the high resistance of the offset region between the gate and drain. Furthermore, anode currents of uncontrolled and offset-TFT-controlled AZO NW FEAs can be modelled by the FN equation, expressed as[22]

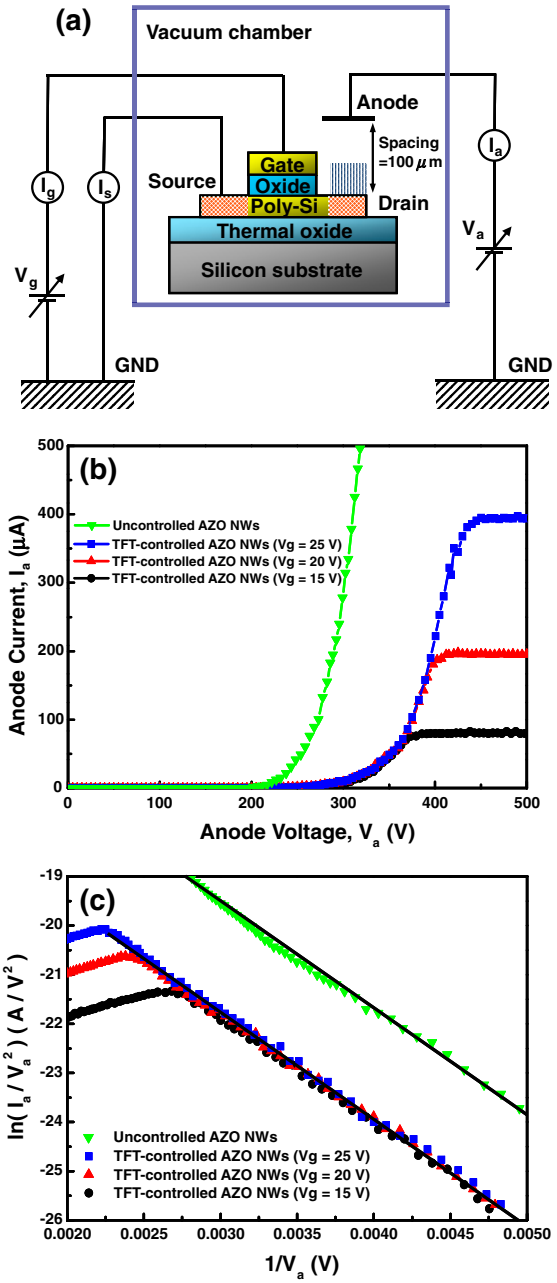

Fig. 5. (Color online) (a) Schematic diagram of a high-vacuum field emission measurement for offset-TFT-controlled AZO NW FEAs. (b) Field emission characteristics of the uncontrolled and offset-TFT-controlled AZO NW FEAs for different gate voltages. (c) Corresponding FN plots of the uncontrolled and offset-TFT-controlled AZO NW FEAs.

$$J = \left(\frac{a\beta^2 E^2}{\varphi}\right) \exp\left(\frac{-B\varphi^{3/2}}{\beta E}\right), \quad (1)$$

where J denotes the current density (A/m^2), E is the applied field, $a = 1.56 \times 10^{-10}\,A{\cdot}eV/V^2$, $B = 6.83 \times 10^9\,V/(m{\cdot}eV^{3/2})$,[23] φ stands for the work function (eV), and β is the field-enhancement factor. Obeying FN theory, a linear relationship between $\ln(I_a/V_a^2)$ and $1/V_a$ can be defined as

$$\ln\left(\frac{I_a}{V_a^2}\right) = \ln\left(\frac{Aa\beta^2}{\varphi d^2}\right) - \frac{Bd\varphi^{3/2}}{\beta}\frac{1}{V_a}, \quad (2)$$

where V_a indicates the applied anode voltage, d represents the distance between the anode and the top surface of the

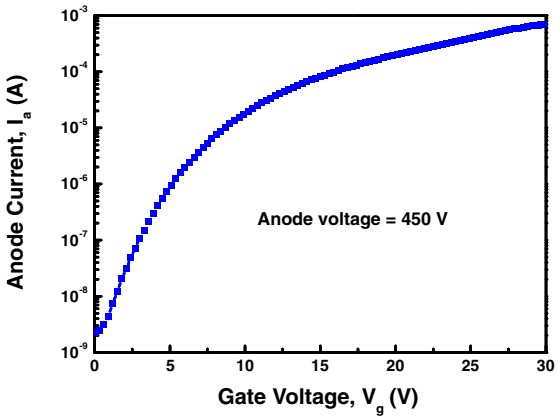

Fig. 6. (Color online) Anode current and gate voltage characteristics of the offset-TFT-controlled AZO NW FEAs.

AZO NWs, and A is the emission area. Figure 5(c) shows the FN plots of $\ln(I_a/V_a^2)$ versus $1/V_a$ for uncontrolled and offset-TFT-controlled AZO NW FEAs. The FN plot of anode current for uncontrolled AZO NW FEAs exhibits a linear dependence within the whole measured range, indicating consistency with FN theory. Fundamentally, the work function of AZO nanostructures can be assumed to equal to that of ZnO, i.e., 5.4 eV,[24] and the β of uncontrolled AZO NW FEAs was determined to be as approximately 3131. On the other hand, transitions of $\ln(I_a/V_a^2)$ versus $1/V_a$ can be observed for offset-TFT-controlled AZO NW FEAs; this is a different FE behavior from that of uncontrolled AZO NW FEAs. When the V_a is low (the large value of $1/V_a$), an approximately linear fitting is found for the plots of $\ln(I_a/V_a^2)$ versus $1/V_a$, suggesting that the anode current is dominated by FN theory at lower anode voltages. As V_a is increased, the transitions of $\ln(I_a/V_a^2)$ versus $1/V_a$ appear, and the fitted slopes changed from negative to positive. When V_a was sufficiently high, a smooth fit with a positive slope of $\ln(I_a/V_a^2)$ versus $1/V_a$ is seen. The positive slope can be associated with the pinch-off of offset-TFTs, resulting in the saturated anode current [revealed in Fig. 5(b)] and the electron supply of AZO NW FEAs being limited by offset-TFTs. Thus, we conclude that the FE behavior of AZO NW FEAs can be controlled by offset-TFTs.

Figure 6 shows the anode current and gate voltage characteristics of the offset-TFT-controlled AZO NW FEAs. The offset-TFT had a channel width (W) of 100 μm and a channel length (L) of 20 μm with an offset length of 15 μm. The anode voltage was kept at 450 V. A large on/off current ratio of 3.05×10^5 was achieved for gate voltage (V_g) switching from 0 to 30 V, indicating that the driving voltage of AZO NW FEAs can be significantly suppressed.

Current stability is a key issue for field emission devices to be applied to flat panel displays. Figure 7 shows the anode current stability of the uncontrolled AZO NW FEAs and offset TFT-controlled AZO NW FEAs over an operating period of one hour. The current fluctuation was defined as $\Delta I/I_{ave}$ ($\Delta I = I_{max} - I_{min}$) under constant applied anode voltage, where ΔI is the variation of the maximum anode current (I_{max}) and the minimum anode current (I_{min}), and I_{ave} is the average anode current. It is apparent that the uncontrolled AZO NW FEAs show a larger current

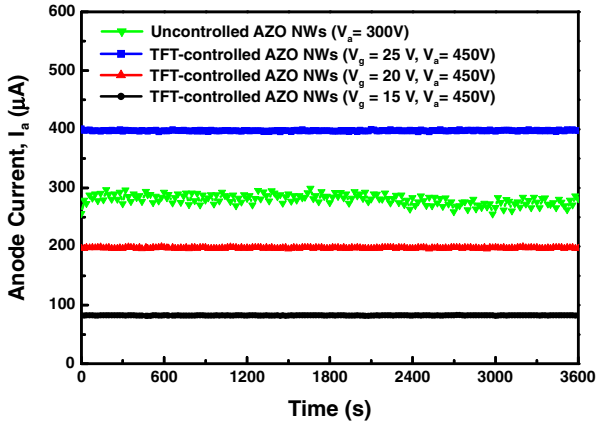

Fig. 7. (Color online) Anode current stabilities of uncontrolled and offset-TFT-controlled AZO NW FEAs over an operating period of one hour.

fluctuation of about 15.6%. In contrast, all stress conditions exhibit very stable emissions achieved via offset-TFT control. The different current levels of offset-TFT-controlled AZO NW FEAs depend upon the different gate voltages. Essentially, the current fluctuation of offset-TFT-controlled AZO NW FEAs was less than 2%. This result indicates that the offset-TFT-controlled AZO NW FEAs can have significantly improved the field emission stability.

4. Conclusions

A new field emission (FE) device composed of a high-voltage offset thin-film transistor (offset-TFT) and Al-doped ZnO (AZO) nanostructure field emitter arrays (FEAs) has been demonstrated. The morphology of AZO nanostructures grown hydrothermally at 85 °C reveals nanowires (NWs). The AZO NW is a single-crystal wurtzite structure with an elongated *c*-axis along the [001] direction of the ZnO crystal. The anode current (I_a) of uncontrolled AZO NW FEAs increased markedly with the anode voltage (V_a). AZO NW FEAs demonstrates superior FE characteristics (i.e., turn-on field of ~2.17 V/μm and threshold field of ~3.43 V/μm) compared with those of conventional CNT FEAs. However, the uncontrolled AZO NW FEAs show a larger current fluctuation of 15.6%. Hence, the architecture of offset-TFT-controlled AZO NW FEAs was studied to suppress the current fluctuation. In addition, the process of low-temperature hydrothermal AZO NWs without plasma damage is beneficial for the stability of offset-TFTs. Offset-TFTs with a 15 μm offset length were chosen considering the balance between the breakdown voltage and I_a. The FE behavior can be controlled by offset-TFTs. A large on/off current ratio of 3.05×10^5 was achieved for a gate voltage (V_g) of 0–30 V. In contrast, the current fluctuation of offset-TFT-controlled AZO NW FEAs was less than 2%, suggesting potential applications in field emission devices and high-brightness electron sources.

Acknowledgements

The authors thank the National Science Council of the Republic of China for their support under Contracts 98-2218-E-009-004 and 99-2221-E-009-168-MY3. Thanks are also due to Chi Mei Optoelectronics Corporation (CMO), the Nano Facillity Center (NFC) in National Chiao Tung University, and the National Nano Device Laboratory (NDL) for technical support.

1) Z. S. Wu, S. Z. Deng, N. S. Xu, J. Chen, J. Zhou, and J. Chen: Appl. Phys. Lett. **80** (2002) 3829.
2) J. M. Bonard, C. Mirko, K. Christian, K. Ralph, N. Olivier, and W. Nicolas: Carbon **40** (2002) 1715.
3) Y. H. Lee, C. H. Choi, Y. T. Jang, E. K. Kim, and B. K. Ju: Appl. Phys. Lett. **81** (2002) 745.
4) Y. F. Zhukovskii, A. I. Popov, C. Balasubramanian, and S. Bellucci: J. Phys.: Condens. Matter **18** (2006) S2045.
5) W. A. de Heer, A. Châtelain, and D. Ugarte: Science **270** (1995) 1179.
6) W. Z. Li, S. S. Xie, L. X. Qian, B. H. Chang, B. S. Zou, W. Y. Zhou, R. A. Zhao, and G. Wang: Science **274** (1996) 1701.
7) P. G. Collins and A. Zettl: Appl. Phys. Lett. **69** (1996) 1969.
8) J. M. Bonard, J. P. Salvetat, T. Stöckli, W. A. de Heer, L. Forró, and A. Châtelain: Appl. Phys. Lett. **73** (1998) 918.
9) S. Kanemaru, T. Hirano, K. Honda, and J. Itoh: Appl. Surf. Sci. **146** (1999) 198.
10) H. C. Cheng, W. K. Hong, F. G. Tarntair, K. J. Chen, J. B. Lin, K. H. Chen, and L. C. Chen: Electrochem. Solid-State Lett. **4** (2001) H5.
11) R. C. Smith, J. D. Carey, R. J. Murphy, W. J. Blau, J. N. Coleman, and S. R. P. Silva: Appl. Phys. Lett. **87** (2005) 263105.
12) T. Unagami and O. Kogure: IEEE Trans. Electron Devices **35** (1988) 314.
13) M. Hack, A. Chiang, T. Y. Huang, A. G. Lewis, R. A. Martin, H. Tuan, I. W. Wu, and P. Yap: IEDM Tech. Dig., 1988, p. 252.
14) T. Unagami: IEEE Trans. Electron Devices **35** (1988) 2363.
15) R. C. Wang, C. P. Liu, J. L. Huang, and S. J. Chen: Appl. Phys. Lett. **88** (2006) 023111.
16) L. Vayssieres: Adv. Mater. **15** (2003) 464.
17) C. J. Lee, J. Park, S. W. Han, and J. Ihm: Chem. Phys. Lett. **337** (2001) 398.
18) S. J. Oh, J. Zhang, Y. Cheng, H. Shimoda, and O. Zhou: Appl. Phys. Lett. **84** (2004) 3738.
19) S. C. Chang, T. C. Lin, and C. Y. Pai: Microelectron. J. **38** (2007) 657.
20) K. C. Chen, C. F. Chen, J. H. Lee, T. L. Wu, C. L. Hwang, N. H. Tai, and M. C. Hsiao: Diamond Relat. Mater. **16** (2007) 566.
21) T. Y. Tsai, Y. A. Li, H. C. Su, N. H. Tai, K. C. Chen, S. H. Lee, L. H. Chan, and Y. Y. Chang: Diamond Relat. Mater. **17** (2008) 594.
22) R. H. Fowler and L. W. Nordheim: Proc. R. Soc. London, Ser. A **119** (1928) 173.
23) H. Araki, T. Katayama, and K. Yoshino: Appl. Phys. Lett. **79** (2001) 2636.
24) Q. Zhao, X. Y. Xu, X. F. Song, X. Z. Zhang, D. P. Yu, C. P. Li, and L. Guo: Appl. Phys. Lett. **88** (2006) 033102.